A NEW METHOD FOR SYNTHESIS OF FORSTERITE NANOMATERIALS FOR BIOIMPLANTS

M.A NAGHIU*, #M. GOREA*, F. KRISTALY**, M. TOMOAIA-COTIŞEL*

** Department of Chemical Engineering, Babes-Bolyai University, Faculty of Chemistry and Chemical Engineering, Cluj-Napoca, Romania*
*** Institute of Mineralogy and Geology, University of Miskolc, Egyetemváros, Miskolc, Hungary*

#E-mail: mgorea@chem.ubbcluj.ro

Submitted November 6, 2013; accepted December 18, 2014

Keywords: Magnesium silicates, Biomaterial, Precipitation method, Particle size, Thermal analysis

Nanocrystalline forsterite (Mg_2SiO_4) was synthesized by the precipitation method using $Mg(NO_3)_2{\cdot}6H_2O$, $C_8H_{20}O_4Si$ (TEOS) and sodium hydroxide as pH regulator as starting materials. The thermal behaviour of the mixture was investigated by a MOM derivatograh. According to DTA results the initial crystallization temperature of the forsterite is about 800°C. The powder calcined at 900°C was characterized by X ray diffraction (XRD). The forsterite was noticed as the main crystalline phase besides of small amounts of periclase (MgO). Polycrystalline forsterite with uniform sized particles and spherical shape is evidenced by electronic microscopy (TEM, SEM). Grain size of forsterite powder according to Counter Coulter-type laser granulometer results is in the range of 10 - 42 nm.

INTRODUCTION

Nanomaterials are widely known as the key materials in nanotechnology due to their unique properties including extremely high diffusion rates, increased strength, and high hardness. Consequently, the sintering times and temperatures are reduced in comparison to the conventional coarse grain materials. Their unique size-dependent properties make these materials superior and indispensable in many areas of human activity [1-5].

Magnesium has attracted attention as a class of biodegradable metallic biomaterials. Magnesium and its alloys have been proposed as a new class of biomedical materials for potential application in orthopedics due to their biodegradation characteristics, their elastic modulus being closer to bone than the currently used medical metals and their better comprehensive mechanical properties than those of biodegradable polymers. Their biodegradability in human body is the most remarkable advantage compared to other metallic biomaterials [6]. Because of its functional roles, magnesium is classified as an essential minor element. Many researchers have demonstrated the stimulatory effects of magnesium on the growth of new bone tissues [7].

The compounds in oxide system $MgO\text{-}SiO_2$ (forsterite and enstatite) have also good medical properties, especially forsterite. Enstatite ($MgSiO_3$) has different polymorphs. The stable forms at high and low temperatures are protoenstatite and orthoenstatite, respectively. A stable form, clinoenstatite, can be formed from ortho- or protoenstatite depending on temperature, internal stresses in grains, and grain size [8, 9]. The changes of enstatite structure under different environmental situations can cause volume changes and produce intrinsic stress, which in turn, decrease the mechanical properties of this material in medical application [10-12]. On the contrary, forsterite does not have any volume changes and due to its good biocompatibility, was preferred to study further.

Forsterite (Mg_2SiO_4), named after the German scientist Johann Forster, is used in many important technology including substrates for high-frequency electronics, ceramic-metal seals, the iron and steel industry, tunable lasers [13] and even as a bone implant material. [14] Recently researches have shown that forsterite is a biocompatible material and can be useful as a biomaterial for hard tissue repair. [15]

Many syntheses of magnesium silicates have been reported [16-25]. Forsterite has been synthesized by different methods such as solid-state reaction, polymer precursor method, co-precipitation and sol-gel methods. The hydrolysis of alkoxides metals or the precipitation methods are frequently used for obtaining homogeneous gels that are then processed for obtaining fine ceramics [26].

During the synthesis of forsterite, it is very difficult to avoid the formation of enstatite ($MgSiO_3$) or/and MgO, and thermal treatments up to 1200 - 1600°C are necessary to obtain pure forsterite. The presence of enstatite in forsterite could be detrimental to the high temperature properties of the material because enstatite dissociates into forsterite and a SiO_2-rich liquid at 1557°C [27].

Since the formation of forsterite is recognized to be difficult, the purpose of the present work is to develop a novel, simple, and economical method for the synthesis of forsterite nanopowder from hydrated magnesium nitrate ($Mg(NO_3)_2 \cdot 6H_2O$) and tetraethyl orthosilicate (TEOS- $C_8H_{20}O_4Si$).

EXPERIMENTAL

Preparation of the forsterite nanopowder

The forsterite nanopowder was synthesized *via* precipitation reaction by using hexahydrated magnesium nitrate ($Mg(NO_3)_2 \cdot 6H_2O$, 99.5 % purity, Merck), tetraethyl orthosilicate (TEOS-$C_8H_{20}O_4Si$, Merck) and sodium hydroxide as pH regulators as raw materials. In order to reach forsterite stoechiometry, magnesium nitrate and TEOS were mixed in an initial 2:1 molar ratio.

The flow chart of synthesis of forsterite is presented in Figure 1.

Magnesium nitrate (0.585 mol) was dissolved into 1200 ml distilled water, and then TEOS was added in the needed amount. Sodium hydroxide was further added drop wise to bring the solution to pH 12 when the solution precipitates; the solution was then stirred for 1 hours. The solution is filtered and the filtrate was washed and dried at 100°C. Finally, the dried precipitate is calcined in a laboratory kiln at a temperature of 900°C for 2 hours plateau at the maximum temperature. The heating rate of dried precipitate was 5°C/min.

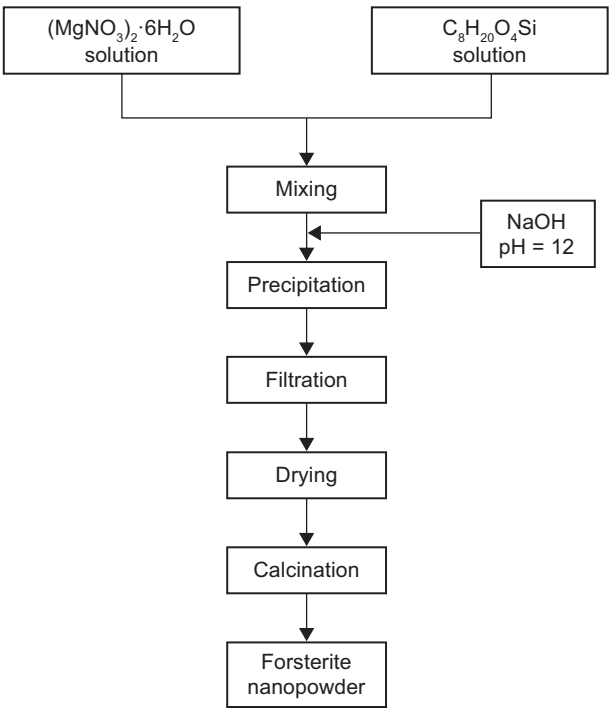

Figure 1. Schematic flow chart of the synthesis of forsterite nanopowder.

Characterisation of the forsterite powder

The diffraction data were collected in the 2θ = = 15 - 85° angular domain with a Bruker D8 Advance diffractometer, using Cu $K\alpha_1$ radiation (λ = 1.5406 A°) (40 kV; 40 mA). In order to increase the resolution, a Ge 111 monochromator was used to eliminate the $K\alpha_2$ radiation.

The crystallite size was estimated from the X-ray diffractograms using the Scherrer formula [27], see Equation 1.

$$D = \frac{k_\lambda}{\beta_{1/2} \cos(\theta)} \quad (1)$$

where: D is the crystallite size (Å); k is a shape factor equal to 0.9; λ is the X-ray wavelength (1.5405 Å); θ is the diffraction angle expressed in radians, and $\beta_{1/2}$ was calculated using equation 2.

$$\beta_{1/2} = \sqrt{B^2 - b^2} \quad (2)$$

B being the diffraction peak width at half height and b = 0.065 the natural width of the instrument. For this purpose, we have selected three individual, very well-differentiated peaks of highest intensity.

The thermal analyses of precursors were carried out using a MOM–C type derivatograph with a heating rate of 10°C/min in a continuous air flow and the temperature was increased up to 1150°C.

A Shimadzu Sald-7101 Counter Coulter laser granulometer was used for investigating the grain size distribution.

The size and morphology of forsterite crystallites were investigated by transmission electron microscopy (TEM) on a JEOL-type JEM 1010 equipment and by scanning electron microscopy (SEM) on a JEOL 5600 LV unit.

RESULTS AND DISCUSSION

Thermal analysis

Differential thermal analyses (DTA) and thermogravimetry (TG) has become the most frequently used characterization method for many materials (composite, fiber, solid waste, nanomaterials and precursors) [28, 29].

Thermogravimetry (TG) and differential thermal analyses (DTA) were performed on the raw mixture

($Mg(NO_3)_2 \cdot 6H_2O$ and TEOS) in the view of investigating the changes occurring during the thermal treatment. The temperature was increased up to 1150°C, when thermal effects and weight losses were recorded. The DTA and respectively TG curves of the studied sample are presented in Figure 2.

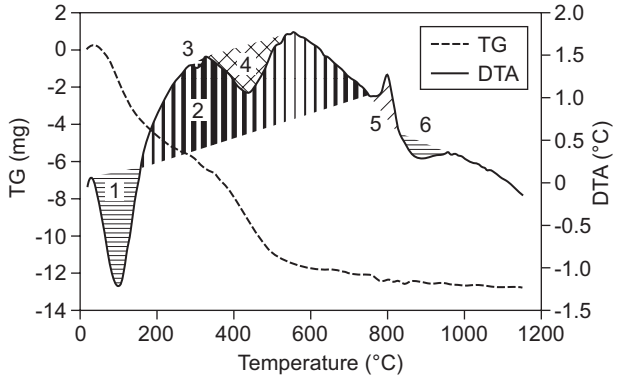

Figure 2. DTA and TG curves of the dried powder.

The thermal effects and weight losses that are observed during the treatment and which are evidenced by DTA and TG curves are presented in Table 1 and Table 2.

The endothermic effect at around 100°C accompanied by 11.71 wt. % weight loss is a result of the removal of adsorbed water present in the precursors due to their hygroscopic nature as well as the partial dehydration of magnesium nitrate. A large peak between 150°C and 770°C is composed from two effects assigned to explosive decomposition of the magnesium nitrate and formation of the magnesium oxide as well as converting of tetraetilorthosilicate (TEOS) in SiO_2 and the oxidation of carbonaceous residues. In this period the loss weight are about 19.65 %. The increase of temperature produces an exothermic peak around 800°C which corresponds to the crystallization of forsterite. The small endothermic effect about 900°C accompanied by 1.85 % weight loss can be assigned to incomplete transformation of TEOS in SiO_2 and continue elimination of OH^- groups. This effect could be explained due to a high heating rate and consequently to a short time for decomposition reaction of TEOS. It observes that this process lasts until 1150°C.

Table 1. Differential thermal effects (DTA) in the studied sample.

Range	1	2	3	4	5	6
T_1 (°C)	57.3	153.5	288.6	330.2	768.6	839.9
T_{max} (°C)	99.1	555	309.8	439.6	798.7	893.3
T_2 (°C)	150.7	767.2	328.8	539.8	837	962.8

Phase composition of the powder

The X-ray diffraction (XRD) pattern of the forsterite powders synthesized at temperature 900°C are shown in Figure 3.

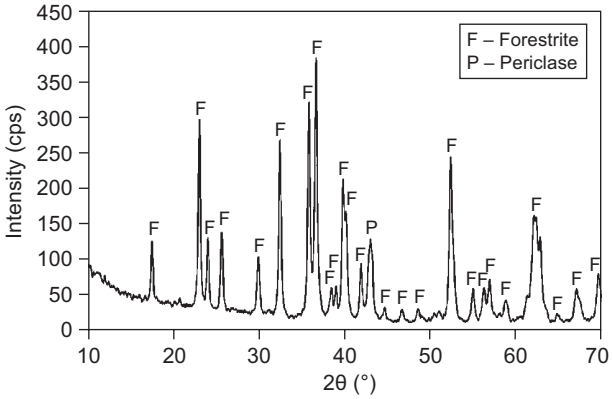

Figure 3. X-ray diffraction pattern of the forsterite synthesized at 900 °C.

According with the thermal analyses data the forsterite crystallizes around the 800°C. Thus, the XRD pattern for samples calcinated at 900°C shows the formation of well crystallized forsterite. Besides the forsterite, a small quantity of periclase, is detected in the sample. The periclase presence could be assigned to an incomplete reaction due to a short time of calcinations or an insufficient homogeneity of the precursor mixture. In case of the fast heating rate, the thermal analyses show a decomposition reaction of precursors till 1150°C. But, a high temperature synthesis will involve an increasing of crystallite size. In previsions article [14] we demonstrated that small amounts of MgO no affected the forsterite biocompatibility. The Si compounds are not detected in XRD pattern, they being under detection limit.

The size of the crystallites in the powders was determined by applying the Scherrer equation. The calculated crystallites size is 19 - 25 nm.

Table 2. Thermo gravimetric effects (TG) in the studied sample.

Range	1	2	3	4	5	6	7	8
T_1 (°C)	54.7	191.3	234.5	343.8	511.2	670.2	729.7	939.6
T_2 (°C)	191.3	233.2	343.8	509.9	640	728.2	935.6	1142.9
TG (%)	11.71	1.4	4.47	11.74	2.04	0.56	1.11	0.74

Grain size distribution

The grain size distribution (cumulative and differential curves) in the forsterite powder is illustrated in Figure 4.

The particle size range is between 10 nm and 42 nm according to crystallite size values calculated by using the Scherrer equation. It can observe that the forsterite powder obtained by precipitation method and calcinated at 900°C is formed from nanosize particles.

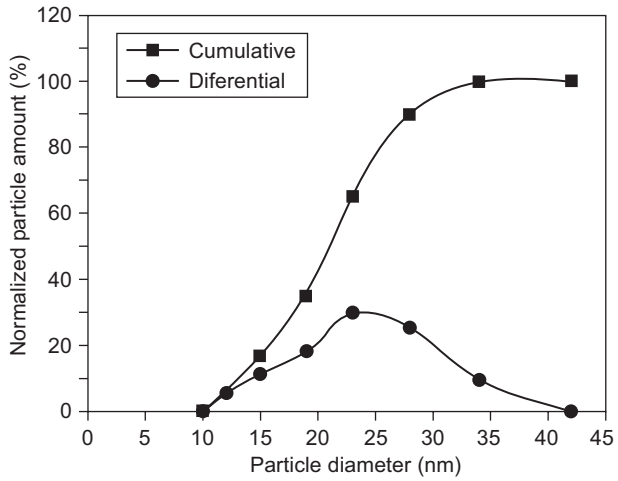

Figure 4. Grain size distribution of forsterite powder.

Electron microscopy

Transmission electron microscopy was used for investigating the morphology and size of the particles in the powder. (Figure 5) The image illustrates that polycrystalline forsterite with uniform sized particles and spherical shape is formed by this process. The crystallite size distribution of the forsterite measured from TEM is in the range 20 - 40 nm according to the previsions tests (grain size test and from XRD pattern).

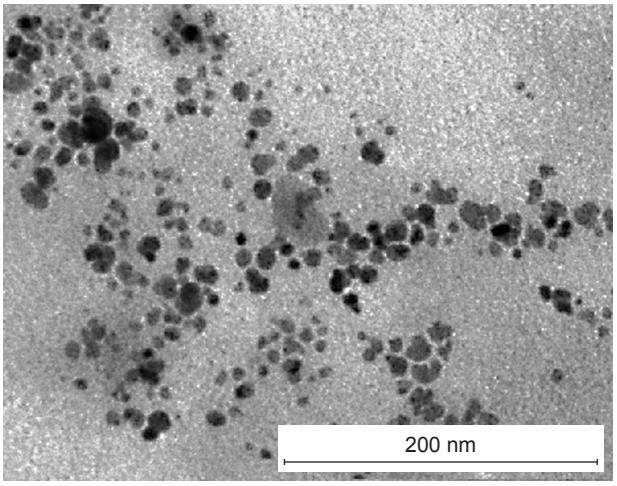

Figure 5. TEM image of forsterite powder

The SEM image of calcined forsterite powder at 900°C is shown in Figure 6. The image illustrates oriental growth of particles. In spite of partial agglomeration, the grain size of powder is in the range of 19 - 45 nm.

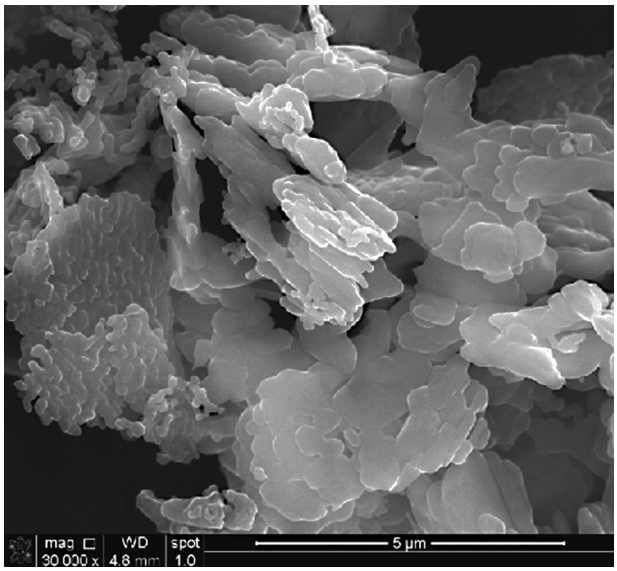

Figure 6. SEM image of forsterite powder.

CONCLUSIONS

Nanocrystalline forsterite (Mg_2SiO_4) was synthesized by precipitation method from hexahydrated magnesium nitrate ($Mg(NO_3)_2 \cdot 6H_2O$), tetraethyl orthosilicate (TEOS-$C_8H_{20}O_4Si$) and sodium hydroxide as pH regulators. The crystallite size of the powder calcined at 900°C is in the range 19 - 25 nm and the particle size is smaller than 45 nm. This chemical synthesis without sucrose and PVA is applicable and produces nanocristaline forsterite powder with compared characteristics to those of other processes of preparing. The crystallization temperature of forsterite is about 800°C according to the thermal analyses data. It is evidenced a uniform sized particles with a weak agglomeration of particles.

Acknowledgment

The authors thank the UEFISCDI for financial support through grant number 171/2012.

References

1. Gorea M., Naghiu M-A., Tomoaia-Cotisel M., Borodi G.: Ceramics – Silikáty *57,* 87 (2013).
2. El-Didamony H., El-Sokkari T. M., Khalil Kh. A., Mohamed Heikal, Ahmed I. A.: Ceramics – Silikáty *56*, 389 (2012).

3. Zhenglong L., Zuyan L., Yanbin C.: Journal of Alloys and Compounds 470 (2009).
4. Tan G.L., Du J.H., Zhang Q.J.: Journal of Alloys and Compounds *468,* 421 (2009**)**.
5. Kharaziha M., Fathi M. H.: Ceramics International, *35*, 2449 **(**2009).
6. X. Lin, L. Tan, Q. Zhang, K. Yang, Z. Hu, J. Qiu, Y. Cai: Acta Biomaterialia (2013) http://dx.doi.org/10.1016/j.actbio.2012.12.016.
7. Xie Y., Zhai W., Chen L., Chang J., Zheng X., Ding C.: Acta Biomaterialia *5*, 6 (2009).
8. Tavangarian F., Emadi R.: Materials Letters *65,* 740 (2011).
9. Huang C.M, Kuo D.H, Kim Y.J, Kriven W.M.: J. Am. Ceram. Soc. *77,* 2625 (1994).
10. Mielcarek W., Nowak-Woźny D., Prociów K.: J. Eur. Ceram. Soc. *24***,** 3817 (2004).
11. Lee W.E., Heuer A.H.: J. Am. Ceram. Soc. *70*, 349 (1987).
12. Sarver J.F, Hummel F.A.: J. Am. Ceram. Soc. *55*, 152 (1962).
13. Lin L., Yin M., Shi C., Zhang W.: Journal of Alloys and Compounds *455***,** 327 (2008).
14. Naghiu M.A., Gorea M., Mutch E., Kristaly F., Tomoaia-Cotisel M.: Journal of Materials Science & Technology *29*, 628 (2013).
15. Mitchell M.B.D., Jackson D., P.F. James: J. Sol-Gel Sci. & Technol. *13*, 359 (1998).
16. Ban T., Ohya Y., Takahashi Y.: J. Am. Ceram. Soc. *82,* 22(1999).
17. Kazakos A., Komarneni S., Roy R.: Mat. Lett. *9*, 405 (1990).
18. Bansal N.P.: J. Am. Ceram. Soc. *71,* 666 **(**1988).
19. Burlitch J.M., Beeman M.L., Riley B., Kohlstedt D.L.: Chem. Mat. *3,* 692 (1991).
20. Jones S.A., Burlitch J.M., Duchamp J.C., Duncan T.M.: J. Sol-Gel Sci. & Technol. *15,* 201 (1999).
21. Martin M.H.E., Ober C.K., Hubbard C., Porter W.D., Cavin O.B.: J. Am. Ceram. Soc. *75,* 1831 (1992).
22. Mitchell M.B.D., Jackson D., James P.F.: J. Sol-Gel Sci. &Technol. *15*, 211 (1999).
23. Echeverrıa L.N.: J. Non-Cryst. Solids *147,* 559 (1992).
24. Douy A.: Journal of Sol-Gel Science and Technology *24,* 221 (2002).
25. Tavangarian F., Emadi R.: Ceramics – Silikáty *54,* 2 (2010).
26. Sanosha K.P., Balakrishnana A., Francisc L., Kima T.N.: J. Alloy. Compd. *495,* 113 (2010).
27. Klug H. P., Alexander L. E.: *X-Ray Diffraction Procedures*, John Wiley & Sons, New York (1974).
28. Iurian A. M., Perhaiţa I., Septelean R., Saponar A.: Studia UBB Chemia *58,* 141 (2013).
29. Popa M., Mesaros A., Mereu R. A., Perhaita I., Ciontea L., Petrisor T.: Studia UBB Chemia *57,* 167 (2012).